Cell

A Mechanical Checkpoint Controls Multicellular Growth through YAP/TAZ Regulation by Actin-Processing Factors

Mariaceleste Aragona,[1] Tito Panciera,[1] Andrea Manfrin,[1] Stefano Giulitti,[2] Federica Michielin,[2] Nicola Elvassore,[2] Sirio Dupont,[1,*] and Stefano Piccolo[1,*]
[1]Department of Molecular Medicine, University of Padua School of Medicine, viale Colombo 3, 35131 Padua, Italy
[2]Department of Industrial Engineering (DII), University of Padua, via Marzolo 9, 35131 Padua, Italy
*Correspondence: dupont@bio.unipd.it (S.D.), piccolo@bio.unipd.it (S.P.)
http://dx.doi.org/10.1016/j.cell.2013.07.042

SUMMARY

Key cellular decisions, such as proliferation or growth arrest, typically occur at spatially defined locations within tissues. Loss of this spatial control is a hallmark of many diseases, including cancer. Yet, how these patterns are established is incompletely understood. Here, we report that physical and architectural features of a multicellular sheet inform cells about their proliferative capacity through mechanical regulation of YAP and TAZ, known mediators of Hippo signaling and organ growth. YAP/TAZ activity is confined to cells exposed to mechanical stresses, such as stretching, location at edges/curvatures contouring an epithelial sheet, or stiffness of the surrounding extracellular matrix. We identify the F-actin-capping/severing proteins Cofilin, CapZ, and Gelsolin as essential gatekeepers that limit YAP/TAZ activity in cells experiencing low mechanical stresses, including contact inhibition of proliferation. We propose that mechanical forces are overarching regulators of YAP/TAZ in multicellular contexts, setting responsiveness to Hippo, WNT, and GPCR signaling.

INTRODUCTION

Spatially restricted patterns of cell proliferation shape embryonic development and maintain adult epithelial tissues. How these local growth patterns are established remains unclear. In the past decades, major emphasis has been placed on graded distribution of soluble growth factors or their restricted activity in "niches." This view, however, does not fully explain how the microenvironment can robustly template cell behavior in time and space with micrometer accuracy (Discher et al., 2009; Huang and Ingber, 1999). Moreover, soluble factors alone can hardly account for some remarkable examples of ordered proliferation, differentiation and self-organization of entire organs emerging in vitro from naive cells cultured in media saturated of mitogens and growth factors (Sasai, 2013). This suggests that tissues are somehow endowed with the capacity to inform individual cells on their proliferative competence, likely including the responsiveness to soluble cues.

Although the molecular nature of these informational systems is uncertain, an intriguing model is that the architectural *form* of the tissue—its shape and three-dimensional geometry—serves as template to initiate and self-sustain asymmetric patterns of cell proliferation (Nelson and Bissell, 2006; Nelson et al., 2005). Key elements of such architectural signal are cell shape, cell geometry, deformation generated by the pulling forces of the extracellular matrix (ECM) and of neighboring cells, and the associated changes in cytoskeletal organization and tension (Berrier and Yamada, 2007; Miranti and Brugge, 2002; Schwartz, 2010; Vogel and Sheetz, 2006). In this model, a specific tissue conformation would translate into a pattern of mechanical forces potentially targeting individual cells with exquisite detail. Supporting this "biomechanical" perspective, the physical properties of the microenvironment are increasingly recognized as potent and pervasive regulators of cell behavior, such as proliferation and differentiation (Halder et al., 2012).

A critical step forward in understanding these processes has been the discovery that mechanical signals are transduced by two related transcriptional coactivators, YAP and TAZ (Dupont et al., 2011). These are powerful regulators of cell proliferation and survival, playing critical roles in organ growth (Pan, 2010; Zeng and Hong, 2008). A number of human cancers hijack these properties to foster their own growth, including induction of cancer stem cells and metastatic colonization (Cordenonsi et al., 2011; Harvey et al., 2013). YAP and TAZ shuttle between the cytoplasm and the nucleus, where they interact with TEAD transcription factors to regulate transcription. Classically, the Hippo cascade has been regarded as the major regulatory input upstream of YAP/TAZ (Pan, 2010). Very recently, WNT and GPCR signaling pathways have also been recognized as important regulators of YAP/TAZ (Azzolin et al., 2012; Yu et al., 2012).

Thinking along the connections between tissue architecture, cell mechanics, and YAP/TAZ biology, we asked: is the mechanical regulation of YAP and TAZ translating spatial force distribution into patterned growth within multicellular layers? If so, how is positional information transmitted to YAP/TAZ? Are the different inputs feeding on YAP/TAZ (e.g., mechanical stimulation, Hippo, WNT, or GPCR signaling) parallel or interdependent regulations?

Here, we started to shed light on these issues by discovering that cell proliferation in an epithelial monolayer is profoundly influenced by a mechanical and cytoskeletal checkpoint that regulates YAP and TAZ. This tissue-level checkpoint is enforced by the F-actin-capping and -severing proteins CapZ, Cofilin, and Gelsolin. These factors inhibit YAP and TAZ in cells that, within a monolayer, are located at sites of low mechanical stress. Conversely, YAP/TAZ-mediated proliferative competence occurs in cells that exhibit higher contractility in response to stretching forces, depending on the shape of the epithelial sheet or on the rigidity of the surrounding ECM. We propose that mechanical stresses are overarching regulators of YAP/TAZ in multicellular contexts, also setting cell responsiveness to Hippo, WNT, and GPCR signaling.

RESULTS

Mechanical Regulation of Cell Proliferation through YAP/TAZ

A classic paradigm on the control of proliferation in multicellular aggregates is contact inhibition of proliferation (CIP), a process by which cultured cells stop dividing when they become confluent occupying the entire space allotted to them. This behavior recapitulates the proliferative arrest of most epithelia, typically leading to cell differentiation or death. Interestingly, loss of CIP is considered a hallmark of cancer (McClatchey and Yap, 2012; Zeng and Hong, 2008). In CIP, a unifying theme is the regulation of YAP and TAZ, which tend to remain nuclear in cells growing at low density and relocate in the cytoplasm in confluent cultures (Zhao et al., 2007). CIP is associated with phosphorylation of YAP and TAZ, indicating the activation of the Hippo pathway kinases (Zhao et al., 2007). However, the regulation of YAP/TAZ by contact inhibition appears more complex. For example, recent data show that, at least in MEFs or keratinocytes, the mammalian Hippo homologs MST1/2 and LATS1/2 are dispensable for CIP (Schlegelmilch et al., 2011; Zhou et al., 2009).

Here we decided to explore a different scenario, in which CIP incorporates a mechanical regulation of YAP and TAZ. To test this, we compared immortalized human mammary epithelial cells (MEC) plated at different densities (3,000, 15,000, and 75,000 cells/cm^2) (Figure 1A). At the lowest plating density (hereafter called ''sparse''), cells exhibited no or minimal contact between neighboring cells. At the intermediate plating density (''confluent''), cells were confluent with all-around cell-cell contacts, whereas, at the highest density (''dense''), space constraints caused cells to form a densely packed monolayer. Using anti-E-cadherin immunofluorescence to identify cell borders, we quantified that the projected cell area dropped more than 10-fold with increasing density, from 1,400 μm^2 in sparse cells to 700 μm^2 in confluent cells and down to 130 μm^2 in dense cells (Figure 1A). As measured by BrdU incorporation, confluent cultures displayed about a 30% reduction of S phase entry when compared to sparse cultures (Figure 1B). This degree of proliferative inhibition is in agreement with the expected contribution of cell-cell contact and E-cadherin engagement to CIP (Kim et al., 2011) and was paralleled by a partial YAP/TAZ cytoplasmic relocalization (Figure 1C). That said, both nuclear YAP/TAZ levels and proliferation remained clearly evident in confluent cultures (Figures 1B and 1C), with YAP/TAZ activity being causal for S phase entry (Figure 1B). This suggests that cell-cell contact per se is not sufficient to induce either postconfluence inhibition of proliferation or robust YAP/TAZ inactivation. This is in contrast to the cells seeded at high density (dense), which are overtly growth arrested and exhibit largely cytoplasmic, transcriptionally inactive YAP/TAZ (Figures 1B and 1C and Figure S1A available online). CIP is reversible, as inducing a ''wound'' in the monolayer by scraping away a stripe of cells caused the cells lying within a few cell diameters from the edge of the wound to stretch without losing cell-cell contacts, relocalize YAP/TAZ to the nuclei, and proliferate (Figure S1B and data not shown). Similar results were observed by using immortalized human HaCaT keratinocytes (Figures S1C–S1F and data not shown).

YAP/TAZ inactivation in the course of CIP has been associated with activation of cell-cell adhesion machinery and activation of the Hippo pathway (Zhao et al., 2007). We thus asked whether the distinct degrees of YAP/TAZ inactivation observed in confluent and dense cultures were dependent on catenins and LATS. Consistent with previous reports (Kim et al., 2011; Schlegelmilch et al., 2011), knockdown of α-catenin, p120-catenin, or LATS1/2 rescued YAP/TAZ transcriptional activity in confluent cultures, as measured by the expression of YAP/TAZ target genes *CTGF*, *CYR61*, and *ANKRD1* (Figures S1G–S1I and data not shown). Surprisingly, however, the same depletions had marginal effects on YAP/TAZ signaling in dense cultures (Figures S1G–S1I).

The above results suggest that, aside from cell-cell contacts, the main determinant for YAP/TAZ inhibition and postconfluent growth arrest is actually to attain a small cell size, intended as adhesion to a small ECM substrate area (Figure 1A). Indeed, cells attaching to a small area are known to experience low mechanical stresses, as they display decreased integrin-mediated focal adhesions, reduced actin stress fibers, and blunted cell contractility (Berrier and Yamada, 2007; Schwartz, 2010; Vogel and Sheetz, 2006). Importantly, these mechanical cues have recently been shown to be essential for YAP/TAZ nuclear localization and activity (Dupont et al., 2011; Wada et al., 2011). In this perspective, CIP would represent the response to a mechanical constraint: as cell crowding progressively boxes individual cells into smaller areas, these would be subjected to the same YAP/TAZ-regulating mechanotransduction pathways that affect isolated cells plated on small ECM islands. In line with this view, MEC plated as single cells on micropatterned fibronectin islands of defined areas displayed strong inhibition of YAP/TAZ nuclear levels and BrdU incorporation when individual cell size dropped below 300 μm^2 (Figures 1D and 1E), independent of cell-cell contacts. Similarly, decreasing mechanical cues by culturing cells on soft substrates (i.e., fibronectin-coated acrylamide hydrogels) also caused cell rounding, YAP/TAZ nuclear exclusion, and proliferative inhibition (Figures 1F, 1G, and S1J). The remarkable phenotypic similarities between cells cultured in small, soft, or dense conditions clearly suggest that these apparently different modalities to regulate YAP/TAZ may actually all correspond to the control of YAP/TAZ by mechanical cues.

To address more directly the notion that, in a multicellular layer, the control of YAP/TAZ activity and cell proliferation occurs

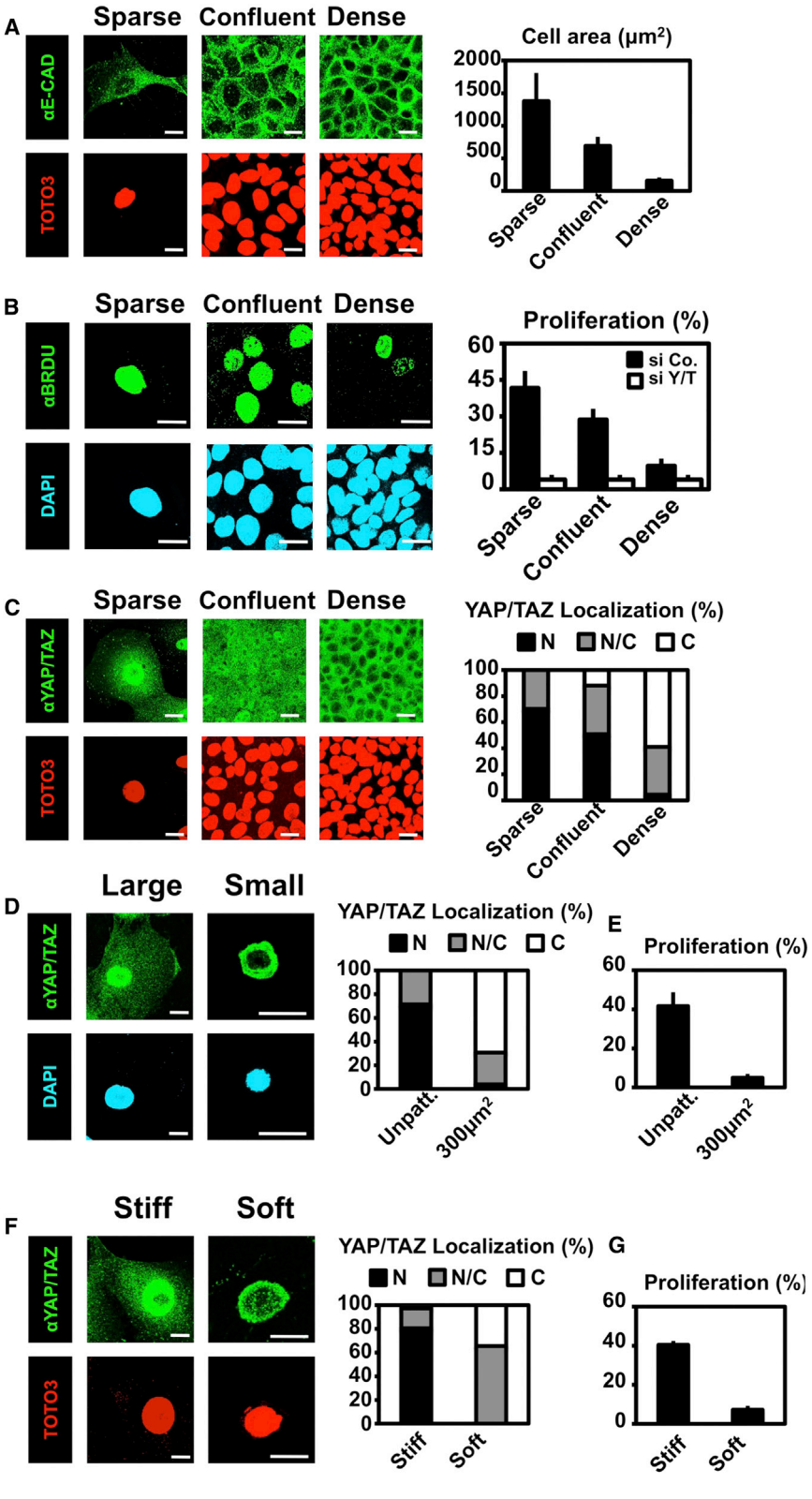

Figure 1. High Cell Density, Small Cell Geometry, and Soft ECM All Lead to Restriction of Cell Area, YAP/TAZ Relocalization, and Growth Arrest

(A) Cells plated at different densities display increasingly smaller cell-substrate adhesion areas. MECs were seeded to obtain sparse cells and confluent or dense monolayers. After 2 days, cells were fixed for immunofluorescence with anti-E-cadherin antibody (αE-CAD) to visualize formation of cell-cell contacts by confocal microscopy. TOTO3 is a nuclear counterstain. Scale bar, 20 μm. (Right) Average cell area in the three seeding conditions. Similar results were obtained with HaCaT keratinocytes (Figure S1C).

(B) MECs were plated as in (A); after 2 days, cells were incubated for 1 hr with a pulse of BrdU to label cells undergoing DNA duplication. Cells were fixed and processed for anti-BrdU immunofluorescence (αBRDU). (Right) Quantitation of proliferation measured as the percentage of BrdU-positive cells. Similar results were obtained with HaCaT keratinocytes (Figure S1D). Note minimal residual proliferation in dense cells, even after YAP/TAZ depletion, suggesting that cell proliferation in culture may not be totally dependent on YAP/TAZ.

(C) MECs were plated as in (A) and stained for immunofluorescence with anti-YAP/TAZ antibody (αYAP/TAZ). TOTO3 is a nuclear counterstain. Scale bar, 20 μm. (Right) Proportion of cells displaying preferential nuclear YAP/TAZ localization (N, black), even distribution of YAP/TAZ in nucleus and cytoplasm (N/C, gray), or cytoplasmic YAP/TAZ (C, white). Similar results were obtained with HaCaT keratinocytes (Figure S1E) and with an independent anti-YAP antibody (not shown).

(D and E). Restricting cell-substrate adhesion area to levels comparable to those of dense cells is sufficient to cause YAP/TAZ nuclear exclusion and inhibition of proliferation. MECs were seeded as individual cells plated on fibronectin-coated glass (large) or on square microprinted fibronectin islands of 300 μm^2 (small). In (D), cells were fixed after 1 day for immunofluorescence with anti-YAP/TAZ antibody (αYAP/TAZ). DAPI is a nuclear counterstain. Scale bar, 20 μm. (Right) YAP/TAZ nucleo/cytoplasmic localization was scored as in (C). In (E), cells were processed for BrdU incorporation as in (B).

(F and G) Effects of a soft ECM substrate on epithelial proliferation. Confocal immunofluorescence images of YAP/TAZ of MECs plated on fibronectin-coated stiff (plastic) and soft (acrylamide hydrogels of 0.7 kPa) substrates. TOTO3 is a nuclear counterstain. Scale bar, 20 μm. On the right: YAP/TAZ nucleo/cytoplasmic localization was scored as in (C). In (G) cells were processed for BrdU incorporation as in (B). Similar results were obtained using acrylamide hydrogels of 40 kPa or plastics (Dupont et al., 2011 and data not shown). Data are mean and SD. Experiments were performed at least three times with three biological replicates each time. Quantitations were carried out by scoring at least 2,000 cells for each sample. Pictures show representative results. See also Table S1 for siRNA sequences and Figure S1.

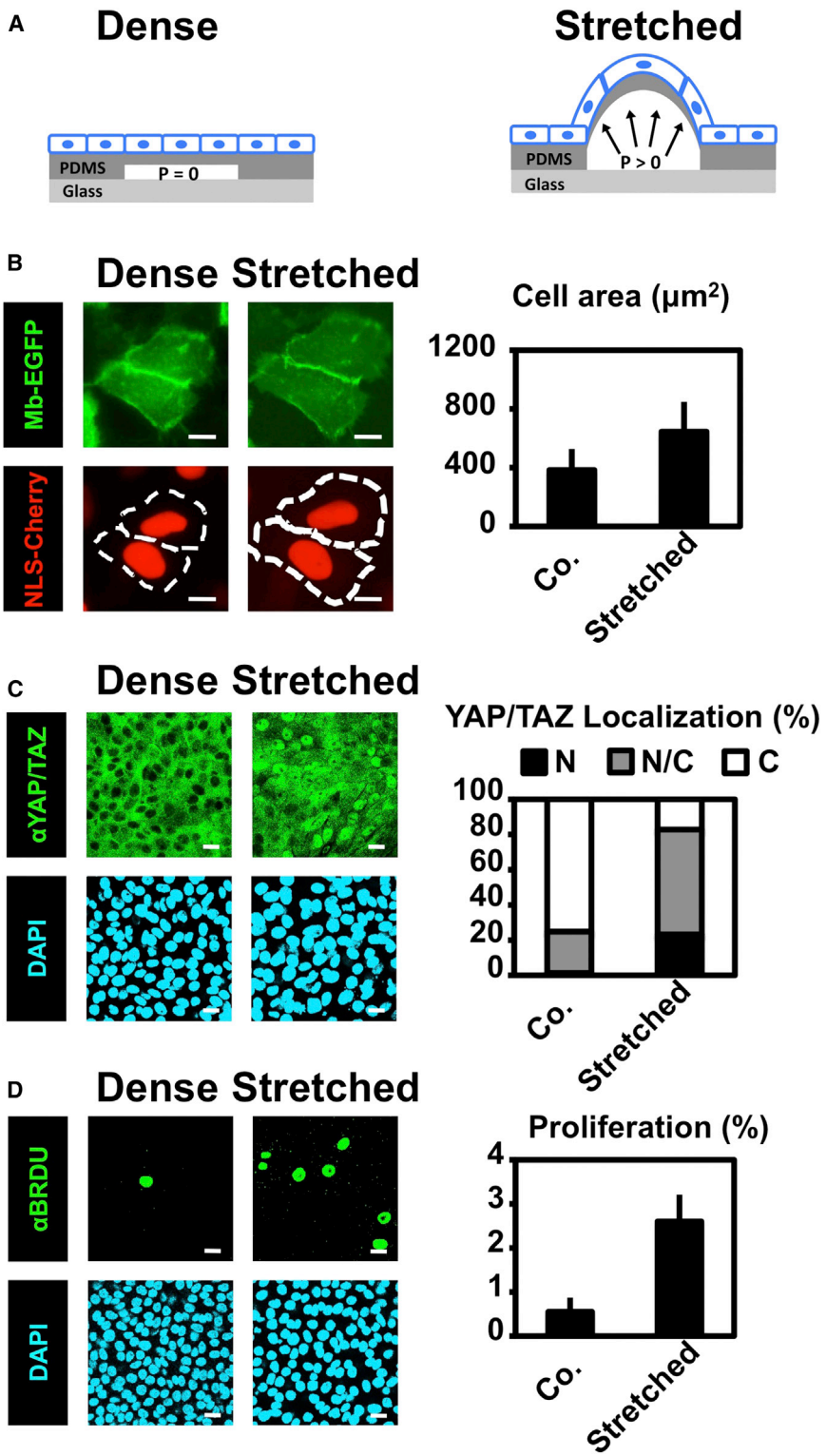

Figure 2. Stretching of an Epithelial Monolayer Overcomes YAP/TAZ Inhibition and Growth Arrest in Contact-Inhibited Cells

(A) A monolayer stretching device. Cells were seeded on the upper surface of a PDMS substrate to obtain a dense monolayer (see also Figure S2A). Underneath the PDMS is a chamber filled of fluid (white space between the PDMS and glass). At atmospheric pressure (dense, p = 0), the cell monolayer remains flat; when pressure is applied to the fluid inside the chamber (stretched, p > 0), the increase of the chamber volume causes a corresponding increase of the surface to which the monolayer is attached.

(B) MECs stably expressing membrane-bound EGFP (Mb-EGFP) and nuclear-localized mCherry (NLS-Cherry) were seeded at dense conditions as in Figure 1A on top of the stretching device. After 2 days, cells were imaged under the epifluorescent microscope before (Co.) and immediately after stretching. Pressure was then maintained constant during observation. Projected cell area was measured in the two conditions (dashed lines in the lower pictures indicate the cell boundaries before and after stretching). The graph shows the average quantitation of cell area. The ramping of pressure increase was set in order to avoid destruction of cell-cell contacts (as monitored with Mb-EGFP; data not shown). Scale bar, 20 μm.

(C) MECs were plated on the stretching device as in (B). After 2 days, cells were subjected to 6 hr of static stretching, fixed with the device still under pressure, and then processed for immunofluorescence with anti-YAP/TAZ antibody (αYAP/TAZ). DAPI is a nuclear counterstain. Scale bar, 20 μm. (Right) Proportion of cells displaying preferential nuclear YAP/TAZ localization (N, black), even distribution of YAP/TAZ between the nucleus and the cytoplasm (N/C, gray), or prevalently cytoplasmic YAP/TAZ (C, white). Similar results were obtained after 3 hr of stretching (not shown).

(D) MECs were plated on the stretching device as described in (B). After 2 days, cells were subjected to 6 hr of static stretching in the presence of BrdU to label cells undergoing DNA duplication. Scale bar, 20 μm. (Right) Quantitation of proliferation measured as the percentage of BrdU-positive cells.

Throughout the panels, data are mean and SD. Experiments were performed at least three times with at least three biological replicates each time. Quantitations were carried out by scoring at least 2,000 cells for each sample. Pictures show representative results. See also Figure S2.

through mechanical cues, we developed a microdevice that reproduces some of the mechanical challenges experienced by tissues, such as stretching (Figures 2A and S2A–S2C). This microdevice was built by fabricating into polydimethylsiloxane silicone (PDMS) a microfluidic network of hollow channels connecting larger "chambers" filled with saline solution. The surface of PDMS was coated with ECM (fibronectin) to allow cell attachment. MECs were seeded on this surface at high cell density,

causing cells to exclude YAP/TAZ from nuclei and undergo CIP. Next, we slowly applied computer-controlled pressure to the system, imposing cells to radially stretch as the PDMS membrane overlaying each chamber inflated (Figure 2A). This applied strain increased the cell adhesive surface to 150%, as quantified from measurements of the cell-projected area (Figure 2B). This was associated to a remodeling of the F-actin cytoskeleton with appearance of phalloidin-positive actin bundles in stretched cells (Figure S2D). Remarkably, stretched cells rapidly reactivated YAP/TAZ, as monitored by nuclear localization, and re-entered S phase (Figures 2C and 2D). Based on these experiments, we conclude that mechanical forces acting on specific areas of an epithelial sheet reflect into changes of shape and mechanics of the individual cells and act as spatially localized determinants of cell proliferation through YAP/TAZ regulation.

F-Actin-Capping and -Severing Proteins Are YAP/TAZ Inhibitors

We next sought to identify molecular players involved in YAP/TAZ regulation by mechanical cues. F-actin regulatory proteins appeared as ideal candidates: treatments that disrupt F-actin or cytoskeletal contractility oppose YAP/TAZ function (Dupont et al., 2011; Wada et al., 2011; Zhao et al., 2012); then, it is recognized that cells respond to external mechanical cues by adjusting the tension and overall organization of their actin cytoskeleton by engaging a plethora of actin-binding proteins (Berrier and Yamada, 2007). Finally, cells plated on small ECM islands, on soft ECM, or in a dense monolayer are characterized by similar F-actin organization, as they retain cortical F-actin, but all display reduced or absent F-actin bundles (Figure S2D and data not shown).

We thus reasoned that knockdown of endogenous negative regulators of F-actin should restore cytoskeletal structures required for YAP/TAZ activity in inhibitory mechanical conditions. We selected a total of 62 genes identified as F-actin inhibitors in a genome-wide screen (Rohn et al., 2011). In order to specifically identify genes relevant for YAP/TAZ regulation by mechanical cues, we screened them using an unambiguous mechanotransduction assay—that is, the rescue of YAP/TAZ-dependent transcription on soft ECM substrates. MECs were transfected with two pairs of siRNAs for each F-actin inhibitor and seeded on soft hydrogels (approximating an elastic modulus of 0.7 kPa). Cells were harvested after 48 hr and were analyzed by quantitative PCR (qPCR) for *CTGF* mRNA expression as readout of YAP/TAZ activity (Figure 3A). Although most siRNAs were ineffective, few siRNAs reactivated *CTGF* expression to levels comparable to or higher than those of cells growing on a stiff matrix (Figure 3B). These candidates were then validated by using individual siRNAs and testing their effectiveness at activating multiple YAP/TAZ endogenous targets (*CTGF*, *ANKRD1*, *CYR61*); among the candidates, Cofilin1/2, Capzb, and Gelsolin, well-established organizers of F-actin distribution and dynamics (Pollard and Cooper, 2009), stood out as potent YAP/TAZ inhibitors (Figures 3C and S3A and data not shown).

Cofilin and Gelsolin (also known as actin-depolymerizing factors) increase the turnover of F-actin by severing microfilaments; after severing, Gelsolin remains attached to the newly formed barbed end, preventing filament annealing and polymerization. CapZ (also known as β-actinin or capping protein) shares with Gelsolin such actin-capping function (Pollard and Cooper, 2009). Most of what we know about Cofilin, Gelsolin, and CapZ in mammalian cells is based on cell migration studies, particularly in the context of dynamic cell protrusions, or from in vitro studies (Pollard and Cooper, 2009), though little data is available on their role in other relevant biological processes.

In sparse MECs, depletion of Cofilin, CapZ, and Gelsolin caused a general increase in F-actin staining, with particularly thickened stress fibers and increased peripheral protrusions resembling filopodia and lamellipodia (Figures 3D and S3B). Supporting the notion that F-actin-capping and -severing proteins do work through F-actin modification to regulate YAP/TAZ, we found that CapZ depletion could not increase YAP/TAZ activity in cells treated with LatrunculinA, an F-actin inhibitory drug (Figure S3C). To further dissect which subset of the F-actin networks is relevant for YAP/TAZ activity, we treated cells with chemical inhibitors of formins (SMIFH2) or ARP2/3 (CK666, CK869; see Supplemental Information for details): these compounds preferentially inhibit formation of F-actin bundles (formin dependent) or of F-actin branched networks that sustain lamellipodia formation (ARP dependent). qPCR for *CTGF* indicated that YAP/TAZ activity mostly depends on F-actin bundles (Figure 3E). Taken together, the results link mechanical regulation of YAP/TAZ activity to F-actin-capping/severing proteins and formation of stress fibers.

We next used F-actin-capping/severing proteins as tools to further query the nature of YAP/TAZ inhibition by cell density. Depletion of Cofilin, CapZ, or Gelsolin rescued formation of stress fibers as well as YAP/TAZ nuclear localization, TAZ protein stability, and YAP/TAZ-dependent gene expression in dense cells (Figures 4A–4C, S4A, and S4B). These findings support the notion that control of YAP/TAZ by high cell density entails a mechanical and cytoskeletal regulation.

Role of YAP/TAZ and F-Actin Inhibitors in Mechanical Patterning of Cell Proliferation

Next, we wondered whether YAP/TAZ reactivation by depletion of F-actin capping and severing proteins is also paralleled by a rescue of CIP. To address this question, we employed microfabrication methods to stamp fibronectin-coated substrates of defined shape and area. This set-up allows studying how patterns of mechanical forces generate patterned growth within a monolayer: cells located at the borders of the island experience higher mechanical stress than cells located in the center (Nelson et al., 2005). MECs were uniformly seeded at high density on circular islands, and after 48 hr, cell proliferation rate was assayed by BrdU incorporation (Figure S4C). As shown in Figure 4D, the number of cells in S phase greatly decreased in the center of the island but persisted at the border, matching the distribution of physical forces (Nelson et al., 2005). Knockdown of YAP and TAZ revealed that proliferation at the border was YAP/TAZ dependent (Figure 4D). This growth pattern—as previously noticed (Nelson et al., 2005)—was driven by tensional forces, as inhibition of nonmuscle myosin II with blebbistatin or of myosin light-chain kinase with ML-7 greatly reduced proliferation at the culture borders, phenocopying attenuation of YAP/TAZ

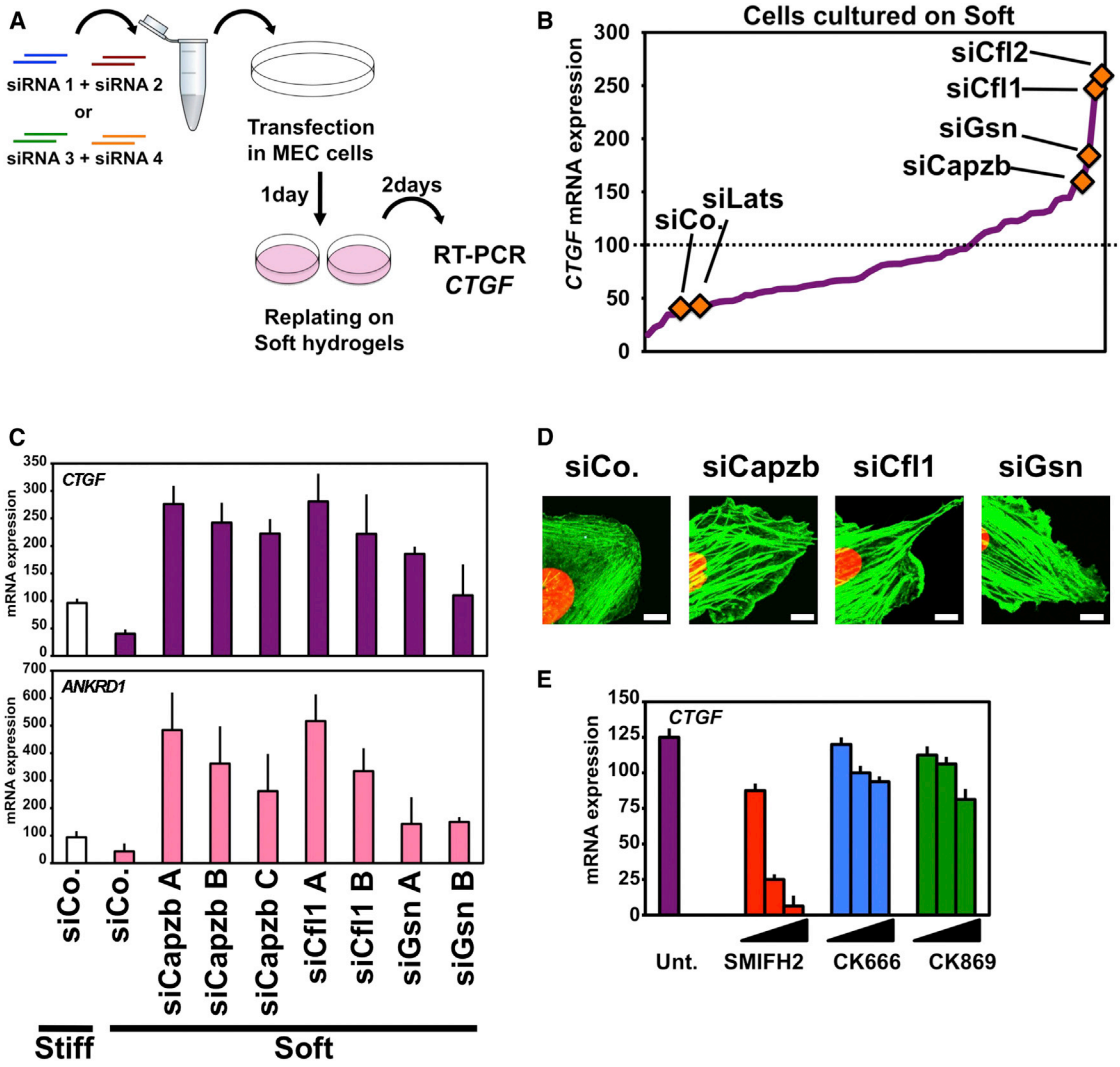

Figure 3. CapZ, Cofilin, and Gelsolin Inhibit YAP/TAZ Activity

(A and B) siRNA screen for negative regulators of the F-actin cytoskeleton impinging on YAP/TAZ activity. (A) Schematic overview of the screening procedure. MECs were transfected with two independent couples of siRNAs against each gene (siRNA 1+2 or siRNA 3+4). The day after transfection, cells were replated as single cells on a soft ECM hydrogel (0.7 kPa) and harvested after 2 more days for qPCR analysis. (B) Results of the screening, where each point of the purple line corresponds to a single siRNA/gene. The orange diamonds indicate the effects of controls and of selected siRNAs that were further validated (see text). Cfl, Cofilin; Gsn, Gelsolin. The dotted line represents *CTGF* levels in cells transfected with siControl (siCo.) but plated on a stiff ECM substrate. Here and throughout the figures, *CTGF* levels are relative to *GAPDH* expression.

(C) Loss of capping and severing proteins rescues YAP/TAZ inhibition on soft ECM. *CTGF* (purple) and *ANKRD1* (violet) expression in MECs are independent readouts of YAP/TAZ transcriptional activity. Cells were transfected with single siRNA against each gene (A, B, or C). Stiff (white column) is a stiff ECM substrate; soft (colored columns) is a 0.7 kPa ECM hydrogel. See Figure S3A for knockdown efficiencies on endogenous proteins.

(D) Loss of Capzb, Cfl1, and Gsn induces formation of thicker actin bundles. Close-up confocal immunofluorescence of MECs transfected with the indicated siRNA and stained for F-actin with phalloidin (green) and nuclei (TOTO3, red). Scale bar, 20 μm. See Figure S3B for increased filopodia and lamellipodia after Capzb, Cfl1, and Gsn knockdown. Consistent results were obtained with independent siRNAs (not shown).

(E) Regulation of F-actin dynamic and assembly by formin proteins is required for YAP/TAZ activity. MECs were plated on a stiff ECM substrate and treated for 24 hr with increasing doses of the inhibitor of formin-homology 2 domains SMIFH2 (used at 5, 15, 30 μM) or of the Arp2/3 inhibitors CK666 (5, 10, 50 μM) and CK869 (5, 10, 50 μM).

Data are mean and SD. Experiments were performed three times with at least three biological replicates each time. See also Figure S3 and Tables S1 and S2.

(Figure 4D). Strikingly, depletion of CapZ and Cofilin clearly prevented CIP in center cells. Importantly, this occurred without increasing the growth of cells at the border, thus partially leveling the growth differentials within the epithelial sheet (Figure 4D). The restoration of proliferation by depletion of capping and severing proteins was dependent on YAP and TAZ (Figure 4D). We obtained similar results by seeding cells on square-shaped islands, where YAP/TAZ-dependent proliferation was

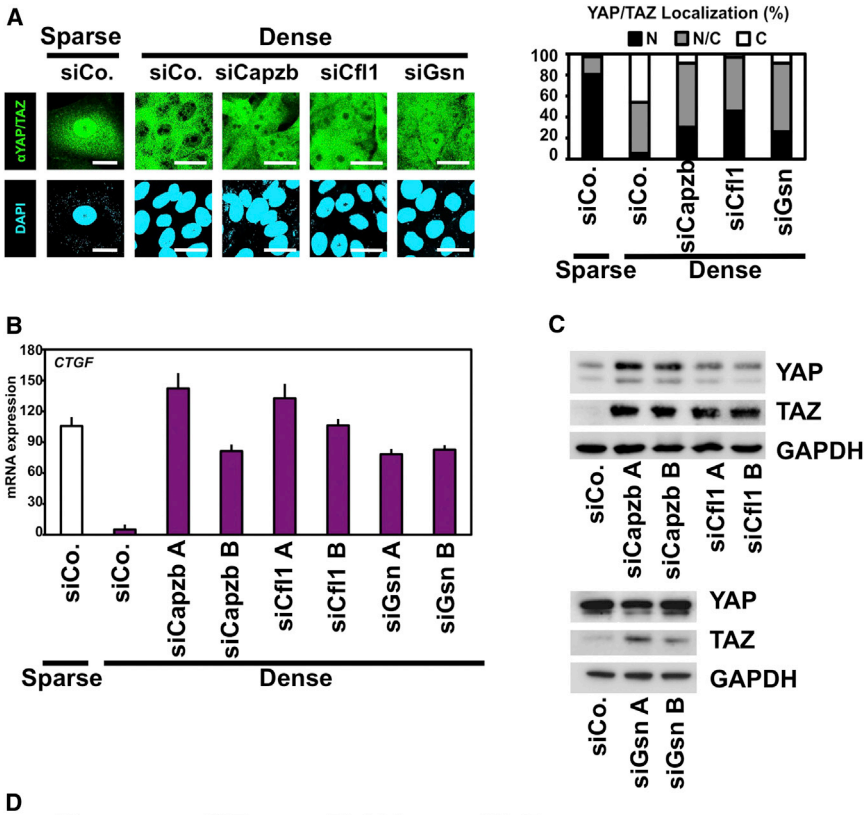

Figure 4. Knockdown of F-Actin-Capping and -Severing Factors Rescues Contact Inhibition of Proliferation

(A) Loss of Capzb, Cfl1, or Gsn rescues YAP/TAZ nuclear localization in dense monolayers. MECs were transfected with the indicated siRNA and were seeded to obtain sparse cells or a dense monolayer. After 2 days, cells were fixed for immunofluorescence with anti-YAP/TAZ antibody (αYAP/TAZ). DAPI is a nuclear counterstain. Scale bar, 20 μm. (Right) Proportion of cells displaying preferential nuclear YAP/TAZ localization (N, black); even distribution of YAP/TAZ between the nucleus and the cytoplasm (N/C, gray); or cytoplasmic YAP/TAZ (C, white). Consistent results were obtained with independent siRNAs (not shown).

(B) *CTGF* expression in MECs transfected and seeded as in (A). Loss of Capzb, Cfl1, and Gsn rescues YAP/TAZ transcriptional activity in dense monolayers.

(C) Western blotting for TAZ and YAP in MECs transfected and seeded as in (A). GAPDH is a loading control.

(D) Panels show colorimetric stacked images of BrdU incorporation, used to visualize spatial variations of proliferation in cell monolayers of defined shape and dimensions. MECs were plated as monolayers on large microprinted fibronectin islands (diameter, 350 μm) and processed as described in the text and as in the Figure S4C legend. The color scale indicates the extent of cell proliferation in a given position of the monolayers. The proliferation rate decreases to nearly undetectable levels at the center of the circle due to CIP (black/blue color), whereas cells continue proliferating along the border of the cellular sheet (green/red color). Cultures were treated with blebbistatin (Blebbi, 50 μM) or myosin light-chain kinase inhibitor (ML-7, 10 μM) overnight before the BrdU pulse. For experiments with siRNAs, cells were first transfected with the indicated siRNA and were replated after 1 day. Similar results were obtained on islands of square shape (Figures S4D and S4E).

Data are mean and SD. Experiments were performed at least twice with biological replicates each time. Quantitations were carried out by scoring at least 2,000 cells for each sample. Pictures show representative results. See also Figure S4 and Table S1.

concentrated at corners and edges (Figures S4D, S4E, and data not shown).

The above results suggest that the form of an epithelial monolayer generates patterns of tensional forces that translate into differentials of YAP/TAZ activity, whose establishment requires F-actin inhibitors. Yet, in vivo, distinct tissues not only exhibit specific shapes, but also their ECM composition varies greatly due to the content, crosslinking, and topology of collagen fibers (Butcher et al., 2009). To mimic such integration, we investigated the roles of YAP/TAZ and F-actin-capping and -severing proteins on the behavior of MECs growing in three dimensions (3D). For this, we used reconstituted ECM containing a mix of basement membrane (BM; Matrigel) and collagenI (COL), whose concentration can be changed to obtain soft and stiff BM/COL gels (COL 1.2 mg/ml or 3 mg/ml, respectively) (Paszek et al., 2005) (see Figure S5A for validation of these gel compositions as mechanoregulators of YAP/TAZ). After 8 days in culture, MECs growing embedded in soft BM/COL gels formed growth-arrested acini (Figure 5A). When collagen concentration was increased, we observed the formation of larger spheroids, actively growing tubules, and organoid-like structures (Figure 5A). By immunofluorescence, YAP/TAZ were predominantly evenly distributed in cells cultured in soft ECMs but were clearly nuclear in cells embedded in the stiffer ECM (Figure 5B). Transcriptional activation of YAP/TAZ by increased ECM stiffness in 3D cultures was confirmed by induction of endogenous markers, such as *CTGF*, *CYR61*, and *ANKRD1* mRNAs (Figure S5B). siRNA-mediated knockdown of YAP and TAZ caused

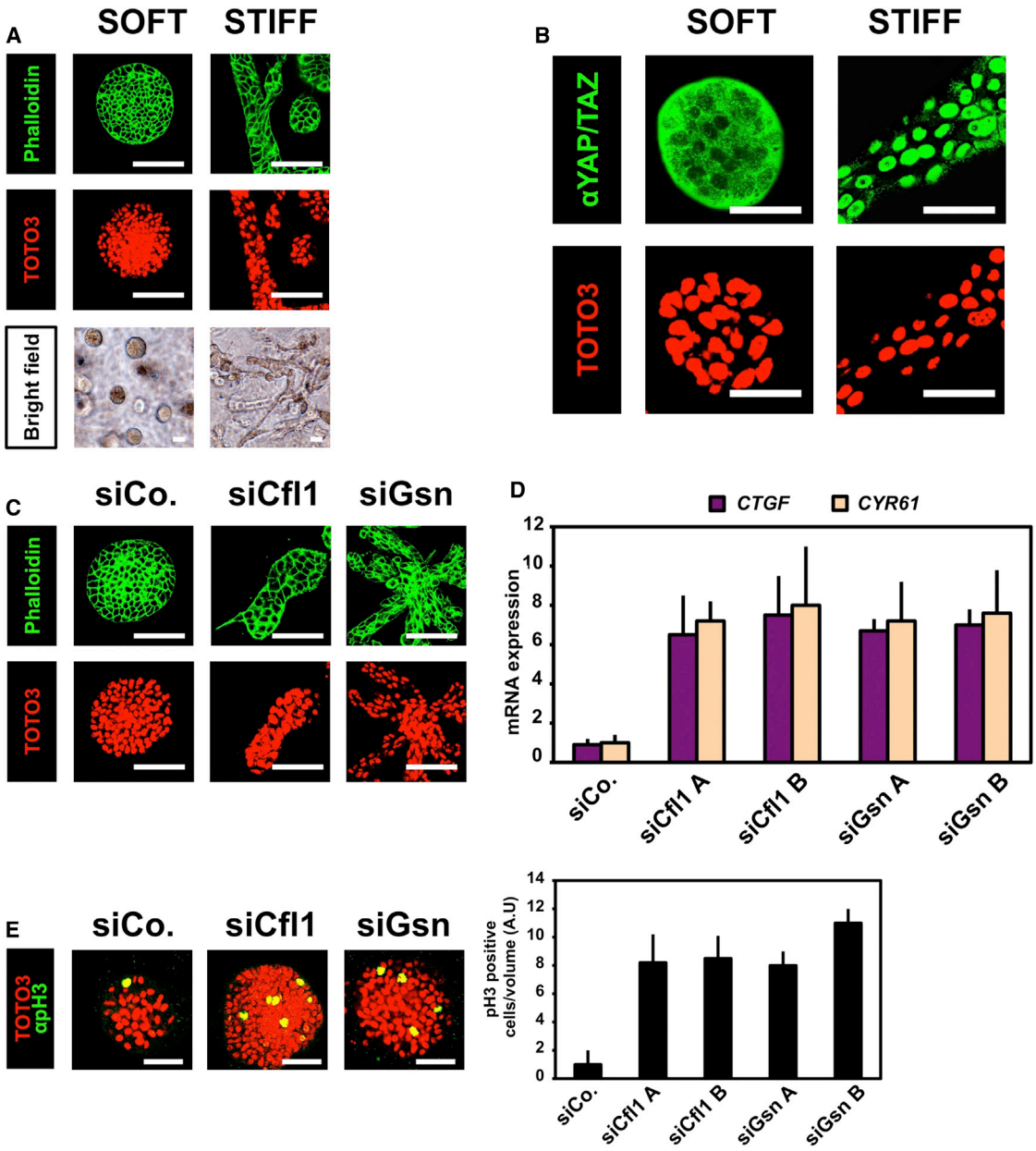

Figure 5. 3D Matrix Stiffness Regulates Growth and Morphogenesis of Mammary Epithelial Cells through YAP/TAZ

(A) Mammary epithelial cells (MECs) were embedded as a single cell in a matrix formed of a different mixture of Matrigel and CollagenI (see Experimental Procedures). Soft matrix contained 1.2 mg/ml CollagenI, whereas stiff matrix contained 3 mg/ml CollagenI (Paszek et al., 2005). After 8 days, cells were fixed and stained for phalloidin to help visualize the morphology of multicellular structures. TOTO3 is a nuclear counterstain. Scale bar, 100 μm. Bottom panels show bright fields at lower magnification.

(B) 3D matrix density regulates YAP/TAZ localization, as assayed by confocal immunofluorescence with anti-YAP/TAZ antibody (αYAP/TAZ). MECs were plated as in (A) and were fixed after 6 days. TOTO3 is a nuclear counterstain. Scale bar, 100 μm.

(C) Loss of Cfl1 and Gsn promotes the formation of tubule-like structures in soft 3D matrix. MECs were transfected with the indicated siRNAs and then embedded in soft matrix as in (A). After 8 days, acini were fixed and stained for phalloidin. TOTO3 is a nuclear counterstain. Scale bar, 100 μm.

(D) Loss of Cfl1 and Gsn increases YAP/TAZ transcriptional activity in soft 3D matrix. MECs were treated as in (C) and were harvested for qPCR of the YAP/TAZ target genes *CTGF* and *CYR61*.

(E) Loss of Cfl1 and Gsn promotes proliferation of cells embedded in 3D soft matrix. MECs were treated as in (C) and were stained with anti-pH3 antibody to mark mitotic cells. pH3 signal is shown merged with the TOTO3 nuclear counterstaining. Scale bar, 100 μm. (Right) Quantitation of cell mitosis normalized to the volume of the multicellular structures, as calculated from 3D z stacks reconstructions. Data are mean and SD obtained from at least 20 structures per condition.

Data are mean and SD. Experiments were performed at least twice with biological replicates each time. Pictures show representative results. See also Figure S5 and Table S1.

severe reduction of the overall number and size of the 3D colonies that in no case expanded beyond small aggregates, regardless of substrate rigidity (data not shown).

We next sustained endogenous YAP/TAZ activity in cells embedded in the soft ECM through siRNA-mediated knockdown of Cofilin or Gelsolin. Strikingly, this induced the formation of bigger acini and caused the appearance of elongated or branched structures (Figure 5C) and was paralleled by YAP/TAZ-dependent induction of *CTGF* and *CYR61* mRNAs (Figure 5D). Using phosphohistone-3 as proliferation marker, acini transfected with control siRNA were mainly growth arrested, whereas Cofilin- or Gelsolin-depleted spheroids retained proliferative activity (Figure 5E). We conclude that YAP/TAZ regulation by F-actin-capping and -severing proteins plays a critical role in regulating the growth of epithelial cells in a 3D reconstituted ECM.

Cytoskeletal Regulation of YAP/TAZ Dominates over Hippo Signaling

We next sought to investigate the intersections between the control of YAP/TAZ activity by cytoskeletal cues and the classical Hippo cascade, centered on the activity of two kinases, MST1/2 (Hippo in *Drosophila*) and LATS1/2, the latter directly phosphorylating YAP/TAZ and causing their inhibition (Pan, 2010). CIP has been associated to increased YAP/TAZ phosphorylation mediated by LATS1/2 (Zhao et al., 2007); similar phosphorylation occurs in cells rounded after placing them in suspension or upon disruption of the F-actin cytoskeleton (Kim et al., 2013; Wada et al., 2011; Zhao et al., 2012). Fully confirming these associations, we also found increased YAP/TAZ phosphorylation in cells treated with LatrunculinA, an F-actin inhibitory drug (Figure 6A). YAP/TAZ phosphorylation, however, may not automatically surrogate for biological function, and no previous studies supported this biochemical observation with functional evidence (Halder et al., 2012). To investigate the functional role of LATS, we used independent pairs of validated siRNAs targeting both LATS1 and LATS2. We first controlled the efficacy of LATS depletion by reconstituting NF2 expression, a bona fide upstream regulator of the Hippo cascade, in the NF2 null breast cancer cell line MDA-MB-231 (Dupont et al., 2011). NF2 re-expression caused a dramatic inhibition of TEAD luciferase reporter, and LATS1/2 inactivation completely abolished this effect, confirming the efficacy of our siRNAs (Figure 6B). Similarly, NF2 re-expression was completely ineffective in cells expressing only a LATS-insensitive, phosphorylation mutant form of YAP or TAZ (Figure S6A and data not shown).

Next, we wondered whether LATS1/2 were downstream of mechanical cues. If this were the case, as in the above NF2 paradigm, loss-of-LATS1/2 or loss-of-YAP/TAZ phosphorylation should also rescue YAP/TAZ activity in cells on soft ECM or dense cultures. In stark contrast to this hypothesis, the results for mechanical regulation were different: depletion of LATS1/2 could not rescue YAP/TAZ inhibition by a soft environment (Figures 6C), indicating that F-actin and mechanical regulation affect YAP/TAZ activity independently of their phosphorylation by LATS. In line, cells expressing only LATS-insensitive YAP or TAZ mutants (5SA-YAP, 4SA-TAZ) did not escape mechanical inhibition when cultured on soft hydrogels (Figures S6B and S6C). Using CapZ inactivation as a paradigm of cytoskeletal remodeling, we also found that cells expressing 4SA-TAZ were still responding to depletion of CapZ (Figure S6D). Finally, knockdown of CapZ left the YAP/TAZ phosphorylation levels completely unchanged, as shown by Phos-TAG analysis (Figure 6D); collectively, the results strongly suggest that YAP/TAZ control by the F-actin cytoskeleton and Hippo signaling represent formally distinct regulations.

An unexpected discovery came when we simultaneously inactivated CapZ together with LATS1/2 in MECs cultured in soft or dense conditions. The results actually showed that LATS1/2 are effective inhibitors of YAP/TAZ only in the context of a mechanically competent F-actin cytoskeleton. Several results support this conclusion: (1) combined depletion of CapZ and LATS1/2 cooperated to fully induce nuclear localization of YAP and TAZ in cells seeded on soft hydrogels and dense conditions (Figures 6E and 6F); (2) LATS1/2 depletion in either soft or dense MEC cultures was inconsequential per se but potently synergized with CapZ depletion to maximize YAP/TAZ transcriptional activity (Figures 6G and 6H); (3) in large square (or round) fibronectin-coated islands, LATS1/2 depletion alone could not rescue CIP (Figures 6I, S6E, S6F) and left proliferation of cells at the border still sensitive to inhibitors of cytoskeletal tension (Figure S6E). However, combined depletion of CapZ and LATS1/2 fully rescued the blockade of S phase entry in cells located at the center of the epithelial sheets, triggering unabated proliferation evenly throughout the island (Figures 6I and S6F).

We next tested how loss of YAP/TAZ regulation by the Hippo kinases impacted MECs growing in 3D within a soft or stiff ECM. To this end, we compared MECs stably expressing near-endogenous levels of wild-type TAZ and LATS-phosphorylation-insensitive 4SA-TAZ. As shown in Figure 6J, wild-type TAZ-expressing cells behaved similarly to their parental counterparts. 4SA-TAZ-expressing cells displayed increased protrusive activity in soft ECM yet retained a spheroid structure. Notably, in the more rigid ECM, 4SA-TAZ-expressing cells did not form tubular structures and invaded the matrix as single cells. As TAZ overexpression has been shown to induce epithelial-to-mesenchymal transition in cells cultured on plastic in 2D (Lei et al., 2008), this 3D phenotype likely reflects fully unleashed TAZ activity.

Finally, we asked whether the permissive effect of the cytoskeleton is specific for the Hippo pathway or also applies to other regulatory inputs. To this end, we used two inducers of YAP/TAZ, WNT and GPCR signaling (Azzolin et al., 2012; Yu et al., 2012), and monitored their efficacy in soft versus stiff extracellular conditions. As shown in Figure 6K, knockdown of APC (mimicking WNT signaling by inactivation of the APC/Axin/GSK3 TAZ destruction complex; Azzolin et al., 2012) caused robust upregulation of YAP/TAZ-dependent transcription in cells cultured on stiff substrates but had minimal effect in cells seeded on a soft matrix. Similarly, addition of TRAP6, a positive inducer of YAP/TAZ activity through GPCR signaling, could operate only in cells cultured on stiff but not soft matrices (Figure 6L). Remarkably, depletion of capping and severing proteins re-empowered YAP/TAZ activation by WNT and GPCR signaling (Figures 6K, 6L, and data not shown). Collectively, the results suggest that

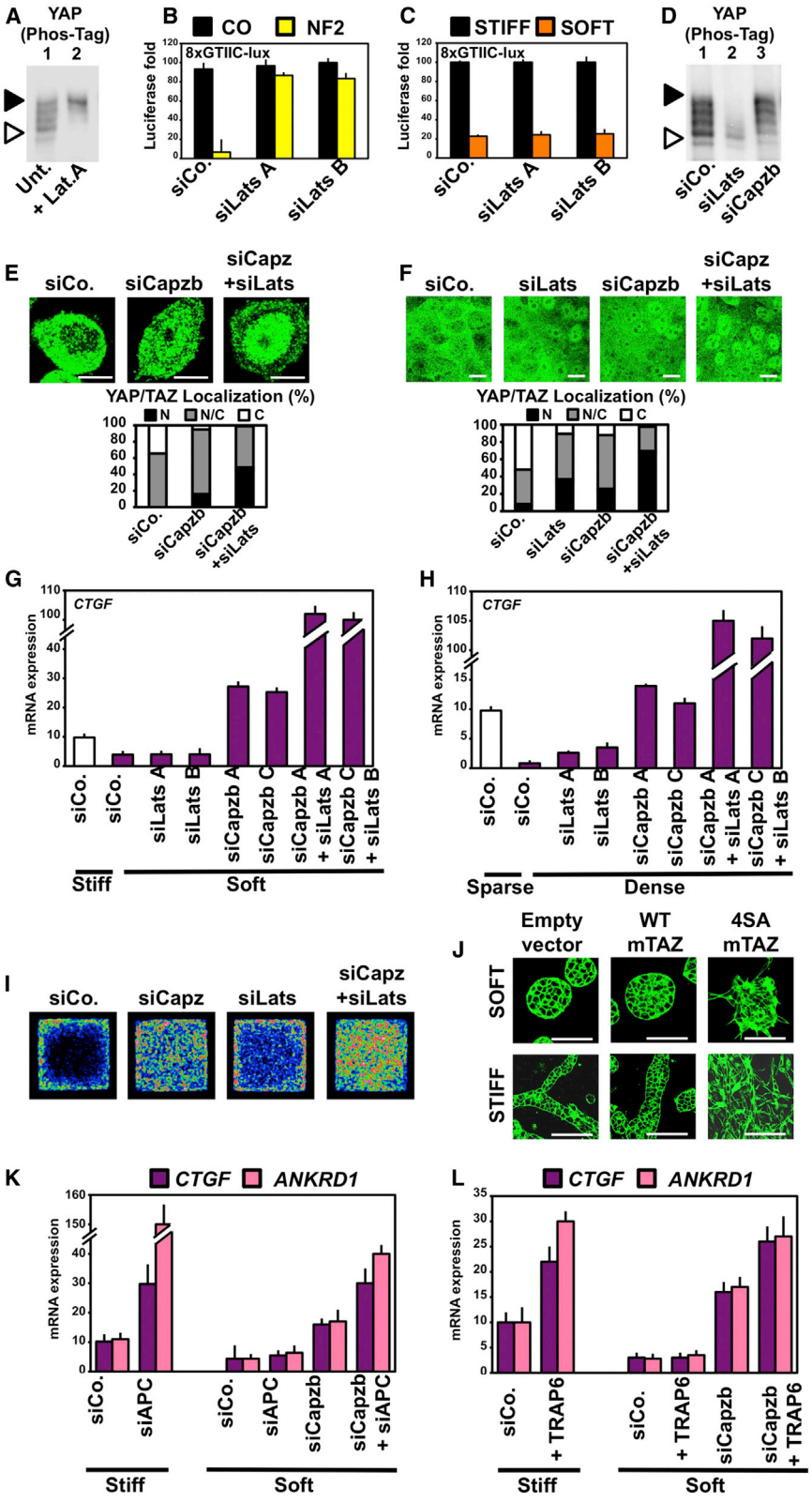

Figure 6. Cytoskeletal Mechanics Is a Dominant Input for YAP/TAZ Activity

(A) Disruption of the F-actin cytoskeleton induces YAP phosphorylation. Phos-TAG SDS-PAGE analysis of MECs plated as confluent monolayer and treated with LatrunculinA (Lat.A, 100 μM) for 3 hr. Black and white arrowheads indicate hyperphosphorylated or nonphosphorylated YAP, respectively. Identity of YAP isoforms was defined based on extracts from cells transfected with YAP siRNA and on λ-phosphatase treatment (not shown).

(B) LATS1/2 knockdown completely rescues YAP/TAZ inhibition by NF2/Merlin. Luciferase reporter assay (8XGTIIC) in MDA-MB-231 transfected with the indicated siRNA and without (Co.) or with NF2 expression plasmid. See Figure S6A for similar results obtained with LATS-insensitive 5SA-YAP mutant. Similar results were obtained in HeLa cells (not shown).

(C) LATS1/2 knockdown does not rescue YAP/TAZ inhibition by soft ECM. Luciferase reporter assay (8XGTIIC) in MDA-MB-231 cells transfected with the indicated siRNA and replated on stiff or soft ECM substrates. See Figure S6B for similar results obtained with LATS-insensitive 5SA-YAP mutant. Similar results were obtained in HeLa cells (not shown). Of note, inhibition of LATS by constitutive-activation of PI3K or AKT (Fan et al., 2013), known for being downstream of integrin signaling, could not rescue YAP/TAZ inhibition by soft ECM; and inhibition of PI3K, AKT, and mTOR by small-molecule inhibitors had no effect on a stiff ECM (data not shown).

(D) Capzb knockdown does not result in a decrease of YAP phosphorylation. Phos-TAG SDS-PAGE analysis of MECs transfected with the indicated siRNAs and plated as confluent monolayers. Black and white arrowheads indicate hyperphosphorylated or nonphosphorylated YAP, respectively.

(E) MECs were transfected with the indicated siRNAs and were plated on soft ECM substrates. After 2 days, cells were fixed for immunofluorescence with anti-YAP/TAZ antibody. Scale bar, 10 μm. (Below the pictures) Proportion of cells displaying preferential nuclear YAP/TAZ localization (N, black), even distribution of YAP/TAZ between the nucleus and the cytoplasm (N/C, gray), or prevalently cytoplasmic YAP/TAZ (C, white). Transfection of LATS1/2 siRNA alone had no significant effects on YAP localization (not shown). Consistent results were obtained with independent siRNAs (not shown).

(F) MECs were transfected with the indicated siRNAs and were seeded to obtain a dense monolayer. After 2 days, cells were fixed for immunofluorescence with anti-YAP/TAZ antibody. Scale bar, 20 μm. (Below the pictures) Proportion of cells displaying preferential nuclear YAP/TAZ localization (N, black), even distribution of YAP/TAZ between the nucleus and the cytoplasm (N/C, gray), or prevalently cytoplasmic YAP/TAZ (C, white).

(G) MECs were transfected with the indicated siRNAs and were plated on stiff (white column) or soft (colored columns) ECM substrates. After

(legend continued on next page)

mechanical and physical properties of the environment control not just Hippo signaling, but also YAP/TAZ responsiveness to signaling cascades initiated by soluble growth factors.

DISCUSSION

How cell shape and tissue form connect with tissue function, growth, and patterning is one of the most fascinating and least understood aspects of biology. Here, we provide evidence that tissue shape and three-dimensional ECM compliance pattern the proliferative competence of an epithelial sheet. These inputs localize YAP/TAZ activity at sites of high mechanical stresses and inhibit it where mechanical forces are minimal. Thus, YAP and TAZ regulation serves as a link between tissue architecture and a key cellular function, proliferation. YAP/TAZ inhibition entails a remodeling of the F-actin cytoskeleton mediated by F-actin-capping and -severing proteins, for which we reveal an essential role as proliferative checkpoints in mammalian epithelial sheets through YAP/TAZ regulation.

The presently described connections appear to hold a number of implications for the biology of epithelial cells. For organ size control, tissue regeneration, and homeostasis, cells must be constantly informed of the size and shape of the whole organ (Discher et al., 2009; Huang and Ingber, 1999; Nelson and Bissell, 2006). This suggests that cells are able to perceive what happens many cell diameters away and respond to it with great spatial accuracy. Mechanical forces are ideally suited to serve as messenger of this global control, as it has been recently shown that forces display long-range and broad-scale effects (Halder et al., 2012; Guo et al., 2012). Using monolayers of defined shape and size, here we show that patterns of mechanical stresses locally control YAP/TAZ activity. At sites of low mechanical forces—that is, in contact-inhibited center cells—YAP/TAZ are inhibited by F-actin-capping and -severing proteins, as loss of CapZ or Cofilin potently rescues YAP/TAZ nuclear localization, transcriptional activity, and proliferation. In contrast, cells at edges and corners of the same multicellular sheets display YAP/TAZ-dependent proliferation induced by cytoskeletal contractility, and here, loss of CapZ or Cofilin has marginal effects.

Inactivation of capping and severing proteins is accompanied by reappearance of F-actin stress fibers. Conversely, YAP/TAZ inactivation is phenocopied by inhibiting formin and myosin, which by themselves are essential for stress fiber formation and cellular contractility. These data collectively suggest that mechanical forces promote YAP/TAZ activity at least in part by inhibiting capping and severing proteins. However, this does not exclude a different scenario, one in which YAP/TAZ are regulated independently by mechanical forces and capping/severing proteins; the latters may operate to unbalance the distribution of microfilaments to different, perhaps competing, F-actin pools (e.g., cortical F-actin, stress fibers, and nuclear actin) endowed with different YAP/TAZ-activating capacities. In other words, though this study unambiguously identifies endogenous F-actin capping and severing proteins as YAP/TAZ inhibitors, a more detailed picture of their function will necessarily require the unraveling of the precise mechanisms by which F-actin affects YAP/TAZ-dependent transcription as well as a more comprehensive understanding of cellular rigidity sensing.

Classical experiments using transformed mammary epithelial cells grown as spheroids in 3D ECM of distinct rigidities and compositions unequivocally showed that the physical properties of the matrix could lead to tumor cell "reversion" to a near normal phenotype, overriding oncogenic aberrations (Nelson and Bissell, 2006). Conversely, ECM stiffening and ensuing cytoskeletal tension cooperate with oncogenes and may even initiate aberrant proliferation (Butcher et al., 2009). Yet, how the physical microenvironment intercepts the malignant phenotype at the level of gene expression is a major question in cancer biology. Here, we show that transformed mammary epithelial cells grown in low-collagen 3D environments display low levels of YAP/TAZ activity, whereas collagen-rich matrices induce YAP/TAZ nuclear localization, YAP/TAZ target genes, and YAP/TAZ-dependent proliferation. These observations are consistent with the positive correlations between collagen content and tissue stiffness (as determined by mammographic density) with breast cancer risk and metastasis (Butcher et al., 2009). Here,

2 days, cells were harvested for qPCR analysis. LATS knockdown has no effects on a soft ECM but potently enhances *CTGF* transcription upon combined depletion of Capzb. Similar results were obtained with *ANKRD1* and *CYR61*.

(H) MECs were transfected with the indicated siRNAs and plated as sparse cells (white column) or dense monolayers (colored columns). After 2 days, cells were harvested for qPCR analysis. Similar results were obtained with *ANKRD1* and *CYR61*.

(I) Combined depletion of LATS1/2 and Capzb completely rescues contact inhibition of proliferation. Panels show colorimetric stacked images of BrdU incorporation in MECs transfected with the indicated siRNAs and seeded on top of microprinted square fibronectin islands (side, 500 μm). The synergistic effect of LATS and Capzb depletion is indicated by the stark increase of red-stained areas (indicating higher proliferation) compared to the other conditions. Similar results were obtained with circular microprinted fibronectin islands (see Figure S6F).

(J) MECs were transfected with YAP/TAZ siRNA (to avoid interference from endogenous proteins) and reconstituted with siRNA-insensitive mouse TAZ (mTAZ). TAZ add-back was carried out with both WT and LATS-insensitive 4SA mTAZ. Cells expressing empty vector and transfected with control siRNA serve as controls. Cells were embedded as a single cell in a matrix formed of a different mixture of Matrigel and CollagenI to obtain softer and stiffer gels (see legend to Figure 5A and Experimental Procedures). After 6 days, cells were fixed and stained for phalloidin to help visualize the morphology of multicellular structures. Scale bar, 100 μm.

(K and L) WNT and GPRC signaling efficiently promote YAP/TAZ-dependent transcription on soft substrates only after Capzb depletion. (K) MECs were transfected with control siRNA (siCo.), APC siRNA (siAPC) to activate WNT signaling, or with Capzb siRNA (siCapzb). Cells were plated on stiff or soft ECM substrates and were harvested after 2 days for qPCR of YAP/TAZ target genes (*CTGF* and *ANKRD1*). (L) MECs were transfected with the indicated siRNAs and were plated on stiff or soft ECM substrates. After 1 day, cells were serum starved overnight and were subsequently left untreated or treated with 2 μM TRAP6 for 3 hr.

Data are mean and SD. Experiments were performed at least twice with biological replicates each time. Quantitations were carried out by scoring at least 2,000 cells for each sample. Pictures show representative results. See also Figure S6 and Table S1.

we show that F-actin-capping and -severing proteins are instrumental for the effects of a soft ECM, as their depletion induces YAP/TAZ activation and proliferation, phenocopying the attributes of a more rigid ECM environment.

This work also provides a unifying principle for how contact inhibition of proliferation is realized. We propose a two-step model of this classic phenomenon (McClatchey and Yap, 2012). As cells engage in cell-cell adhesion—starting from a situation of unrestricted adhesive areas with fully nuclear YAP/TAZ—the E-cadherin/catenin system triggers LATS activation and YAP/TAZ phosphorylation, as previously reported (Kim et al., 2011; Zeng and Hong, 2008), but this is insufficient for overt growth arrest. Then, as proliferation continues, cell crowding causes reduction of cell size and low mechanical stress, now leading to a more effective contact inhibition.

We show that the regulation of YAP/TAZ by cell mechanics is not only distinct from Hippo pathway-induced YAP/TAZ phosphorylation and inhibition but, in fact, dominates over it. Remarkably, LATS1/2 inactivation is per se inconsequential in cells experiencing a low mechanical stress. Moreover, depletion of F-actin-capping/severing proteins sustains YAP/TAZ activity without affecting their phosphorylation. In fact, LATS-mediated inhibition of YAP/TAZ requires a mechanically competent cytoskeleton, as the effect of LATS knockdown becomes manifest only in the absence of F-actin-capping/severing proteins. Our finding that LATS and F-actin organization act independently to regulate YAP/TAZ is also supported by genetic evidence in *Drosophila* (Fernández et al., 2011; Sansores-Garcia et al., 2011). In fly wing development, inactivation of the CapZ homolog induces organ overgrowth similarly to *Hippo* mutations, and the extent of this phenotype can be either counteracted or amplified, respectively, by overexpression or inactivation of LATS, altogether making unlikely an epistatic relationship between the two inputs. Our data further suggest that the scale of activation of YAP/TAZ may be particularly broad, depending on the relative intensity and duration of cytoskeletal and Hippo controls.

There is ample genetic evidence for the Hippo pathway as an intrinsic regulator of organ size; for example, inactivation of the upstream Hippo kinase MST1/2 or of its cofactor Salvador/WW45 causes remarkable tissue overgrowth in several organs, including liver, intestine, and skin (Ramos and Camargo, 2012). According to our findings, the effect of a Hippo pathway mutation should not indiscriminately affect all cells but should preferentially expand the cell populations experiencing a mechanical stress. The existence of a second control layer for YAP/TAZ activity overseeing the effects of an Hippo mutation is supported by in vivo observations: in the liver, YAP/TAZ hyperactivation by Hippo deficiencies generates a functional and histologically well-organized organ (Ramos and Camargo, 2012; Zhou et al., 2009), a finding incompatible with global and uncontrolled cell proliferation. Similarly, in the α-catenin knockout mouse model, YAP activation remains spatially restricted to the basal layer of the skin, where YAP protein is normally confined (Schlegelmilch et al., 2011), suggesting that cell attachment to the appropriate ECM is instrumental to locally sustain normal as well as aberrant YAP activation. Finally, the idea that the cytoskeleton is a key input for YAP/TAZ in vivo is supported by recent genetic evidence: kidney development requires YAP activation by the CDC42 Rho-GTPase, a well-known promoter of F-actin polymerization (Reginensi et al., 2013).

In addition to the Hippo pathway, mechanical cues also dominate the cellular response to soluble cues positively affecting YAP and TAZ activity. We show that YAP/TAZ activation by WNT or GPCR signaling requires a mechanically stressed cytoskeleton or, in cells experiencing a soft ECM, inactivation of F-actin capping and severing proteins. In the same line of thought, the fact that YAP/TAZ are stabilized and act in stem and progenitor cells, typically lodged in specific tissue niches (Ramos and Camargo, 2012), is an enticing argument that the status of the ECM, the cell's cytoskeletal organization, and tension may impart a "physical" competence for stemness and differentiation.

EXPERIMENTAL PROCEDURES

Details are provided in the Extended Experimental Procedures.

Plasmids

siRNA-insensitive FLAG-hYAP1 WT and 5SA were generated by PCR and subcloned in pcDNA3. pXJ40-HA-Merlin/NF2 S518A is Addgene#19701. 8xGTIIC-lux (Dupont et al., 2011) is Addgene#34615.

Cell Cultures and Transfections

MCF10A and MII cells were used with equal results, except for experiments shown in Figures 3 and 5, where we used only MII cells. Micropatterned glass slides were from Cytoo. Fibronectin-coated hydrogels were as previously described (Dupont et al., 2011). The monolayer stretching device was fabricated by using standard soft-lithography techniques. For 3D assays, cells were embedded into mixes of Growth Factor Reduced Matrigel (BD Biosciences) and CollagenI (Trevigen Cultrex 3D Culture Matrix Rat CollagenI). For assays on large square and circular fibronectin-coated islands, one million cells were plated in a 35 mm dish containing a single Cytoo glass slide. siRNA transfections were done with Lipofectamine RNAi-MAX (Life Technologies). Sequences of siRNA are provided in Tables S1 and S2. DNA transfections were done with TransitLT1 (Mirus Bio). siRNA and DNA transfection were performed on sparse cells plated on tissue culture plastics before replating on the various ECM substrates and islands. For retroviral infections, see Azzolin et al. (2012).

Antibodies and Bioassays

Antibodies: anti-YAP/TAZ (sc101199), anti-CAPZB (sc81804), anti-COFILIN1 (Epitomics 6663-1), anti-GELSOLIN (sc57509), anti-GAPDH (Millipore mAb374), anti-LATS1 (CST) and anti-LATS2 (Abcam), and anti-E-Cadherin (BD Biosciences). For microscopy, luciferase, proliferation, and real-time PCR assays, see Extended Experimental Procedures.

SUPPLEMENTAL INFORMATION

Supplemental Information includes Extended Experimental Procedures, six figures, and two tables and can be found with this article online at http://dx.doi.org/10.1016/j.cell.2013.07.042.

ACKNOWLEDGMENTS

We thank Michelangelo Cordenonsi, Francesca Zanconato, Elena Enzo, and Oliver Wessely for thoughtful discussion. This work is supported by AIRC-PI, PRIN-Miur and by a University of Padua grant to S.D. and by AIRC Special Program Molecular Clinical Oncology "5 per mille," HSFP, Excellence-IIT, and Epigenetics Flagship project CNR-Miur grants to S.P.

Received: June 17, 2013
Revised: July 16, 2013
Accepted: July 26, 2013
Published: August 15, 2013

REFERENCES

Azzolin, L., Zanconato, F., Bresolin, S., Forcato, M., Basso, G., Bicciato, S., Cordenonsi, M., and Piccolo, S. (2012). Role of TAZ as mediator of Wnt signaling. Cell *151*, 1443–1456.

Berrier, A.L., and Yamada, K.M. (2007). Cell-matrix adhesion. J. Cell. Physiol. *213*, 565–573.

Butcher, D.T., Alliston, T., and Weaver, V.M. (2009). A tense situation: forcing tumour progression. Nat. Rev. Cancer *9*, 108–122.

Cordenonsi, M., Zanconato, F., Azzolin, L., Forcato, M., Rosato, A., Frasson, C., Inui, M., Montagner, M., Parenti, A.R., Poletti, A., et al. (2011). The Hippo transducer TAZ confers cancer stem cell-related traits on breast cancer cells. Cell *147*, 759–772.

Discher, D.E., Mooney, D.J., and Zandstra, P.W. (2009). Growth factors, matrices, and forces combine and control stem cells. Science *324*, 1673–1677.

Dupont, S., Morsut, L., Aragona, M., Enzo, E., Giulitti, S., Cordenonsi, M., Zanconato, F., Le Digabel, J., Forcato, M., Bicciato, S., et al. (2011). Role of YAP/TAZ in mechanotransduction. Nature *474*, 179–183.

Fan, R., Kim, N.-G., and Gumbiner, B.M. (2013). Regulation of Hippo pathway by mitogenic growth factors via phosphoinositide 3-kinase and phosphoinositide-dependent kinase-1. Proc. Natl. Acad. Sci. USA *110*, 2569–2574.

Fernández, B.G., Gaspar, P., Brás-Pereira, C., Jezowska, B., Rebelo, S.R., and Janody, F. (2011). Actin-Capping Protein and the Hippo pathway regulate F-actin and tissue growth in Drosophila. Development *138*, 2337–2346.

Guo, C.-L., Ouyang, M., Yu, J.-Y., Maslov, J., Price, A., and Shen, C.-Y. (2012). Long-range mechanical force enables self-assembly of epithelial tubular patterns. Proc. Natl. Acad. Sci. USA *109*, 5576–5582.

Halder, G., Dupont, S., and Piccolo, S. (2012). Transduction of mechanical and cytoskeletal cues by YAP and TAZ. Nat. Rev. Mol. Cell Biol. *13*, 591–600.

Harvey, K.F., Zhang, X., and Thomas, D.M. (2013). The Hippo pathway and human cancer. Nat. Rev. Cancer *13*, 246–257.

Huang, S., and Ingber, D.E. (1999). The structural and mechanical complexity of cell-growth control. Nat. Cell Biol. *1*, E131–E138.

Kim, N.-G., Koh, E., Chen, X., and Gumbiner, B.M. (2011). E-cadherin mediates contact inhibition of proliferation through Hippo signaling-pathway components. Proc. Natl. Acad. Sci. USA *108*, 11930–11935.

Kim, M., Kim, M., Lee, S., Kuninaka, S., Saya, H., Lee, H., Lee, S., and Lim, D.-S. (2013). cAMP/PKA signalling reinforces the LATS-YAP pathway to fully suppress YAP in response to actin cytoskeletal changes. EMBO J. *32*, 1543–1555.

Lei, Q.-Y., Zhang, H., Zhao, B., Zha, Z.-Y., Bai, F., Pei, X.-H., Zhao, S., Xiong, Y., and Guan, K.-L. (2008). TAZ promotes cell proliferation and epithelial-mesenchymal transition and is inhibited by the hippo pathway. Mol. Cell. Biol. *28*, 2426–2436.

Luni, C., Michielin, F., Barzon, L., Calabrò, V., and Elvassore, N. (2013). Stochastic model-assisted development of efficient low-dose viral transduction in microfluidics. Biophys. J. *104*, 934–942.

McClatchey, A.I., and Yap, A.S. (2012). Contact inhibition (of proliferation) redux. Curr. Opin. Cell Biol. *24*, 685–694.

Miranti, C.K., and Brugge, J.S. (2002). Sensing the environment: a historical perspective on integrin signal transduction. Nat. Cell Biol. *4*, E83–E90.

Nelson, C.M., and Bissell, M.J. (2006). Of extracellular matrix, scaffolds, and signaling: tissue architecture regulates development, homeostasis, and cancer. Annu. Rev. Cell Dev. Biol. *22*, 287–309.

Nelson, C.M., Jean, R.P., Tan, J.L., Liu, W.F., Sniadecki, N.J., Spector, A.A., and Chen, C.S. (2005). Emergent patterns of growth controlled by multicellular form and mechanics. Proc. Natl. Acad. Sci. USA *102*, 11594–11599.

Pan, D. (2010). The hippo signaling pathway in development and cancer. Dev. Cell *19*, 491–505.

Paszek, M.J., Zahir, N., Johnson, K.R., Lakins, J.N., Rozenberg, G.I., Gefen, A., Reinhart-King, C.A., Margulies, S.S., Dembo, M., Boettiger, D., et al. (2005). Tensional homeostasis and the malignant phenotype. Cancer Cell *8*, 241–254.

Pollard, T.D., and Cooper, J.A. (2009). Actin, a central player in cell shape and movement. Science *326*, 1208–1212.

Ramos, A., and Camargo, F.D. (2012). The Hippo signaling pathway and stem cell biology. Trends Cell Biol. *22*, 339–346.

Reginensi, A., Scott, R.P., Gregorieff, A., Bagherie-Lachidan, M., Chung, C., Lim, D.-S., Pawson, T., Wrana, J., and McNeill, H. (2013). Yap- and Cdc42-dependent nephrogenesis and morphogenesis during mouse kidney development. PLoS Genet. *9*, e1003380.

Rohn, J.L., Sims, D., Liu, T., Fedorova, M., Schöck, F., Dopie, J., Vartiainen, M.K., Kiger, A.A., Perrimon, N., and Baum, B. (2011). Comparative RNAi screening identifies a conserved core metazoan actinome by phenotype. J. Cell Biol. *194*, 789–805.

Sansores-Garcia, L., Bossuyt, W., Wada, K.-I., Yonemura, S., Tao, C., Sasaki, H., and Halder, G. (2011). Modulating F-actin organization induces organ growth by affecting the Hippo pathway. EMBO J. *30*, 2325–2335.

Sasai, Y. (2013). Cytosystems dynamics in self-organization of tissue architecture. Nature *493*, 318–326.

Schlegelmilch, K., Mohseni, M., Kirak, O., Pruszak, J., Rodriguez, J.R., Zhou, D., Kreger, B.T., Vasioukhin, V., Avruch, J., Brummelkamp, T.R., and Camargo, F.D. (2011). Yap1 acts downstream of α-catenin to control epidermal proliferation. Cell *144*, 782–795.

Schwartz, M.A. (2010). Integrins and extracellular matrix in mechanotransduction. Cold Spring Harb. Perspect. Biol. *2*, a005066.

Vogel, V., and Sheetz, M. (2006). Local force and geometry sensing regulate cell functions. Nat. Rev. Mol. Cell Biol. *7*, 265–275.

Wada, K.-I., Itoga, K., Okano, T., Yonemura, S., and Sasaki, H. (2011). Hippo pathway regulation by cell morphology and stress fibers. Development *138*, 3907–3914.

Yu, F.-X., Zhao, B., Panupinthu, N., Jewell, J.L., Lian, I., Wang, L.H., Zhao, J., Yuan, H., Tumaneng, K., Li, H., et al. (2012). Regulation of the Hippo-YAP pathway by G-protein-coupled receptor signaling. Cell *150*, 780–791.

Zeng, Q., and Hong, W. (2008). The emerging role of the hippo pathway in cell contact inhibition, organ size control, and cancer development in mammals. Cancer Cell *13*, 188–192.

Zhao, B., Wei, X., Li, W., Udan, R.S., Yang, Q., Kim, J., Xie, J., Ikenoue, T., Yu, J., Li, L., et al. (2007). Inactivation of YAP oncoprotein by the Hippo pathway is involved in cell contact inhibition and tissue growth control. Genes Dev. *21*, 2747–2761.

Zhao, B., Li, L., Wang, L., Wang, C.-Y., Yu, J., and Guan, K.-L. (2012). Cell detachment activates the Hippo pathway via cytoskeleton reorganization to induce anoikis. Genes Dev. *26*, 54–68.

Zhou, D., Conrad, C., Xia, F., Park, J.-S., Payer, B., Yin, Y., Lauwers, G.Y., Thasler, W., Lee, J.T., Avruch, J., and Bardeesy, N. (2009). Mst1 and Mst2 maintain hepatocyte quiescence and suppress hepatocellular carcinoma development through inactivation of the Yap1 oncogene. Cancer Cell *16*, 425–438.